Moroccan Journal of Chemistry
ISSN: 2351-812X
http://revues.imist.ma/?journal=morjchem&page=login
Azaid & al. / Mor. J. Chem. 10 N°4 (2022) 830-850
DOI: https://doi.org/10.48317/IMIST.PRSM/morjchem-v10i4.34457

The photophysical properties and electronic structures of ((2E, 2'E)-1, 1'-[chalcogen bis (4, 1-phenylene)] bis [3-(4-chlorophenyl) prop-2-en-1-one] derivatives as hole-transporting materials for organic light-emitting diodes (OLEDs). Quantum chemical investigations

A. Azaid[1], T. Abram[1], R. Kacimi[1], M. Raftani[1], A. Sbai[1], T. lakhlifi[1] and M. Bouachrine[1, 2*]

[1]*Molecular Chemistry and Natural Substances Laboratory, Faculty of Sciences, University Moulay Ismail, Meknes, Morocco*
[2]*EST Khenifra, University Sultan Moulay Sliman, Morocco*

** Corresponding author:*
m.bouachrine@umi.ac.ma
Received 02 May 2022,
Revised 27 Aug 2022 ,
Accepted 05 sept 2022

Abstract

In order to propose new organic materials for organic light-emitting diodes (OLEDs) applications, The quantum chemical calculations have been performed on four molecules M0 ((2E, 2'E)-1, 1' (selenobis (4, 1phenylene)) bis (bis (3-(4-chlorophenyl) prop-2en-1-one)), M1 ((2E, 2'E)-1, 1' (thiobis (4, 1phenylene)) bis (bis (3-(4-chlorophenyl) prop-2en-1-one)), M2 ((2E, 2'E)-1, 1' (oxybis (4, 1phenylene)) bis (bis (3-(4-chlorophenyl) prop-2en-1-one)), M3 ((2E, 2'E)-1, 1' (azanediylbis (4, 1phenylene)) bis (bis (3-(4-chlorophenyl) prop-2en-1-one)).The principal objective of this work is to study the effect of Chalcogen (O, S, and Se) and nitrogen (N) on geometrical, electronic, optical, and charge transfer properties of these compounds by setting their ionization potentials (IP), their electron affinities (EA), their chemical reactivity indices, their reorganization energies, their electrostatic potential as well as the nonlinear optical (NLO) properties. The geometry of these studied compounds was obtained after optimization in their fundamental states by using the functional density theory (DFT) with the B3LYP method and the basis set 6-311G (d, p). The studied parameters determined from the most stable conformation of each studied molecule. The time-dependent density theory method TD-DFT-B3LYP 6-311G (d, p) was used for the study of absorption. The results of the theoretical calculations show that the mentioned parameters above are affected by the change of atoms O, S, Se, and NH. The smaller hole and electron reorganization energies of these molecules suggest possible use in OLEDs.

Keywords: *OLEDs, DFT, TD-DFT, Electronic properties, Chalcogen (O, S, and Se) and nitrogen (N)*

1. Introduction

During the past few decades, organic semiconductors materials constitute an important class of materials with remarkable properties leading to a huge field of research in both chemistry and physics [1]. These materials are considered good candidates for optoelectronic applications and especially research on new low cost organic photovoltaic devices [2]. This is due to their specific properties such as high charge mobility, thermal, and photochemical stability [3, 4, 5]. Recall that organic semiconductors materials are already widely used in many organic optoelectronic devices, including organic photovoltaic cells [6], organic phototransistors [7], organic resonant tunnel diodes [8] organic field-effect transistors (OFETs) [9], organic light-emitting diodes (OLEDs) [10]. These electroluminescent devices are of great interest because of their important physicochemical characteristics and are considered the devices of tomorrow [11]. Historically, the electroluminescence of organic molecules has been a well-known phenomenon since the mid-twentieth century [12]. However, the first high-efficiency organic light-emitting diode (OLED) devices have been invented by Tang and VanSlyke in 1987 [13, 14]. Since then, OLED performance has evolved considerably, leading to better results. Organic light-emitting diodes (OLEDs), which are organic luminescent materials made of small molecules and polymers, have been widely used in next-generation, high-quality, flat-panel displays, and solid-lighting applications [15]. As we know, the most common OLED structure generally consists of several layers of organic material between a cathode and an anode, which is often transparent formed of indium-tin-oxide (ITO) [16] (Figure1). A high-performance OLED is composed of several organic materials, such as the injection and charge transport layers (electrons and holes), the hole blocking layer and the emission layer [17]. The fundamental step of the OLED electroluminescence phenomenon is the injection of electrons and holes into the different organic layers from the cathode and the anode, respectively. The luminescence of organic materials is due to the radiative recombination of excitons. Within the framework of improve the efficiency of organic light-emitting materials [18, 19], several works have recently been done, especially the study of short-chain luminescent compounds that can be used in an OLED structure [20].

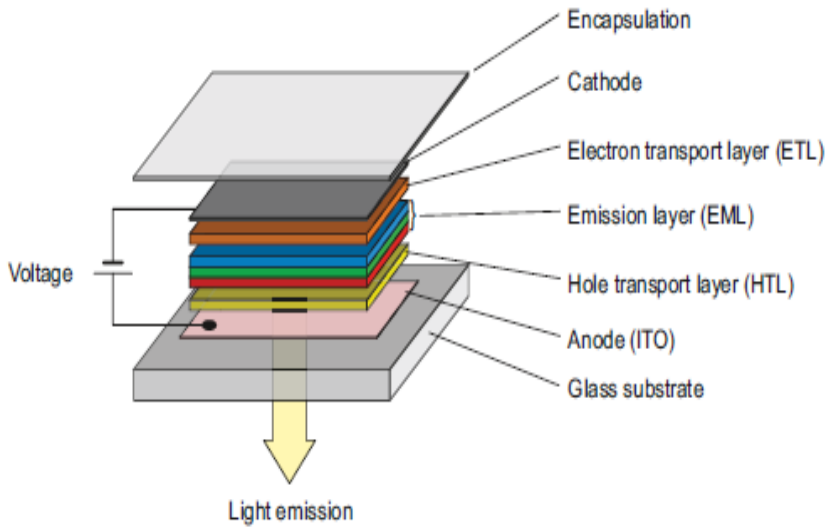

Figure 1. Typical structure of a multilayer OLED with the ITO used as an anode

Recently, a study based on the analysis of the crystal structure and the Hirshfeld surface of (2E, 2'E)-1, 1' (selenobis (4, 1-phenylene)) bis (3-(4-chlorophenyl) prop-2 en-1-one) has been carried out by H. Bouraoui et al [21]. The M0compound characterized by an A-D-A structure has excellent electronic properties and can be useful as high-performance charge-transport materials. The chemical structure of the studied compound studied is shown in Figure. 2. The used A-D-A structure is identified for modulating these electronic properties. The strategy is the use of multiple methods PM6, HF, DFT/B3LYPand DFT/ B3PW91 with the same basis set 6-311G (d, p) to optimize the geometry of our studied compounds. Then, the functional giving the closest geometrical parameters to the experimental ones will

be used in the next quantum calculations of the proposed structures for applications in organic light-emitting diodes (OLEDs). In this study, the quantum chemical calculations have been performed on the proposed structures based on phenylene, Chalcogen (O, S, and Se), and nitrogen (N). The study of the structural and electronic properties of the four studied molecules have been reported: M0 ((2E, 2'E)-1, 1'(selenobis (4, 1phenylene)) bis (bis (3-(4-chlorophenyl) prop-2en-1-one)), M1 ((2E, 2'E)-1, 1'(thiobis (4, 1phenylene)) bis (bis (3-(4-chlorophenyl) prop-2en-1-one)), M2 ((2E, 2'E)-1, 1'(oxybis (4, 1phenylene)) bis (bis (3-(4-chlorophenyl) prop-2en-1-one)), M3 ((2E, 2'E)-1, 1'(azanediylbis (4, 1phenylene)) bis (bis (3-(4-chlorophenyl) prop-2en-1-one)).The principal objective of this work is to study the effect of Chalcogen (O, S and Se) and nitrogen (N) on optical and charge transport properties in the studied compounds. In this context, from the most stable conformation of the studied molecules proposed in Figure 2, both functional density theory (DFT) at B3LYP method with the 6-311G (d, p) basic set and the time-dependent density functional theory TD-DFT-B3LYP/ 6-311G (d, p) have been used to investigate theoretically the geometrical parameters, the optical and electronic properties, ionization potentials (IP), electron affinities (EA), chemical reactivity indices, hole and electron reorganization energies, and electrostatic potential. We hope that the present theoretical study can help to design more materials emitters and to deepen our understanding of the intrinsic excited-state properties of the compound's emitters used in OLEDs devices.

2. Materials and methods

In this work, The Methods PM6, HF, DFT/B3LYPand DFT/ B3PW91have been used with the same basis set 6-311G (d, p) [22]. It is noted that all of these calculations have been performed using the Gaussian 09 package [23]. The geometry structures of neutral molecules (M0, M1, M2 and M3) have been optimized. The energies of the HOMO, LUMO, band gap, chemical reactivity indices and electrostatic potential and nonlinear optical (NLO) properties of these compounds were also determined from the optimized structures. The D-DFT/B3LYP/6-311G (d, p) and TD-DFT/CAM-B3LYP/6-311G (d, p) methods were applied to study electronic properties in the excited state such as UV-visible absorption wave number, corresponding oscillator forces, excitation vertical energy and other related properties.

3. Results and discussion

3.1. Geometrical parameters

The optimized geometry parameters have been performed by theoretical calculations using the PM6, HF, DFT/B3LYP and DFT/ B3PW91 with the same basis set 6-311G (d, p). The comparative optimized structural parameters such as bond lengths, bond angles with its experimental data proposed by H. Bouraoui et al [21] are presented in Table 1 by the atom numbering scheme illustrated in Figure 2. The optimized bond length of C-C is an average of 1.395Å. The bond length of Cl connected with C13 and C28 is 1.741Å and 1.737Å respectively. The bond lengths of the oxygen connected with C7 and C22 are respectively 1.217Å and 1.229 Å, while C-Se bond lengths vary from 1.913Å to 1.916 Å. The computed bond lengths and bond angles are in reasonable agreement with the corresponding experimental values. According to the theoretical values, it can be found out that most of the optimized bond lengths are slightly superior to the experimental values. On the other hand, when comparing experimental bond angles to that of theoretical, the values correlate well with the experimental results of the molecules in the solid phase. There are some deviations when compared with the experimental data, and these differences are probably due to intermolecular or intramolecular interactions in the solid-state [24]. This deviation can also be attributed to the fact that the theoretical calculations were aimed at the isolated molecules in the gaseous phase and the experimental results were aimed at the molecule in the solid-state. Despite these differences, the calculated geometrical parameters represent a good approximation. Indeed, the value of the angle C-Se-C obtained by the functional B3LYP (6-311G (d, p)) (99.3°) are the closest to those measured experimentally (99.0°) (Table 1). So, this method will be used to predict other structures,

taking the molecule studied as a start. The goal is to propose molecules with specific properties for optoelectronic applications.

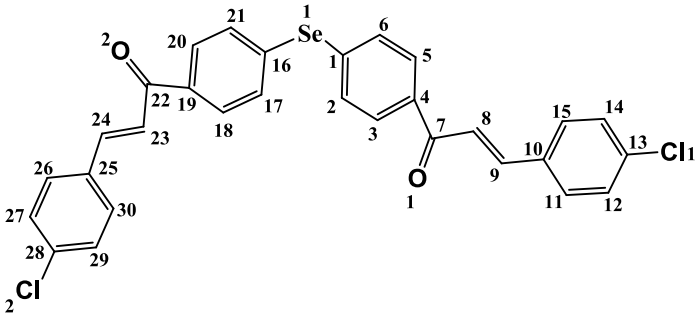

Figure 2. Sketch of chemical structure compound M0

Table 1. ***Experimental and computed bond lengths (Å) and bond angles (°) of molecule M0***

Parameters	Experimental	B3LYP	B3PW91	HF	PM6
Bond length(Å)					
Se1—C1	1.916	1.927	1.922	1.925	1.911
Se1—C16	1.913	1.928	1.920	1.925	1.911
Cl1—C13	1.741	1.754	1.741	1.741	1.724
Cl2—C28	1.737	1.754	1.741	1.741	1.724
O1—C7	1.217	1.228	1.219	1.192	1.213
O2—C22	1.229	1.228	1.219	1.192	1.213
C1—C2	1.376	1.401	1.398	1.391	1.397
C1—C6	1.364	1.397	1.393	1.383	1.399
C2—C3	1.377	1.388	1.384	1.378	1.397
C3—C4	1.386	1.404	1.399	1.392	1.403
C4—C5	1.368	1.401	1.396	1.385	1.401
C4—C7	1.500	1.501	1.497	1.503	1.496
C5—C6	1.398	1.395	1.391	1.387	1.398
C7—C8	1.482	1.482	1.477	1.488	1.490
C8—C9	1.317	1.348	1.343	1.326	1.336
C9—C10	1.462	1.464	1.460	1.476	1.472
C10—C11	1.401	1.408	1.403	1.394	1.405
C10—C15	1.400	1.406	1.401	1.389	1.407
C11—C12	1.380	1.389	1.384	1.378	1.396
C12—C13	1.392	1.397	1.392	1.384	1.396
C13—C14	1.369	1.393	1.388	1.378	1.397
C14—C15	1.362	1.391	1.387	1.384	1.395
C16—C17	1.385	1.396	1.394	1.383	1.399
C16—C21	1.396	1.401	1.397	1.391	1.397
C17—C18	1.383	1.396	1.390	1.387	1.398
C18—C19	1.396	1.401	1.397	1.385	1.401

C19—C20	1.387	1.404	1.399	1.392	1.403
C19—C22	1.477	1.502	1.496	1.503	1.496
C20—C21	1.371	1.388	1.399	1.378	1.397
C22—C23	1.459	1.482	1.478	1.489	1.490
C23—C24	1.325	1.348	1.343	1.326	1.337
C24—C25	1.466	1.464	1.460	1.476	1.472
C25—C26	1.383	1.408	1.403	1.394	1.405
C25—C30	1.395	1.406	1.401	1.389	1.407
C26—C27	1.380	1.389	1.384	1.378	1.396
C27—C28	1.361	1.397	1.392	1.384	1.396
C28—C29	1.387	1.393	1.388	1.378	1.397
C29—C30	1.369	1.392	1.387	1.384	1.395
Parameters	Experimental	B3LYP	B3PW91	HF	PM6
Bond angles (°)					
C1—Se1—C16	99.0	99.3	100.8	100.0	100.0
C2—C1—C6	118.2	119.7	119.8	119.6	120.4
C2—C1—Se1	122.1	121.2	122.2	121.1	122.3
C6—C1—Se1	119.7	119.0	117.82	119.1	117.1
C1—C2—C3	121.5	119.9	119.7	120.0	119.6
C1—C2—H1	119.2	119.7	120.1	120.0	121.6
C3—C2—H1	119.2	120.2	120.0	119.8	118.7
C2—C3—C4	120.0	120.7	120.9	120.6	120.2
C2—C3—H2	120.0	120.8	120.6	120.3	120.3
C4—C3—H2	120.0	118.3	118.3	119.0	119.3
C5—C4—C3	119.0	118.8	118.8	119.0	119.6
C5—C4—C7	122.4	123.3	123.1	122.8	121.8
C3—C4—C7	118.5	117.6	117.8	117.9	118.5
C4—C5—C6	120.0	120.5	120.5	120.4	120.1
C4—C5—H3	120.0	120.0	120.0	120.3	120.1
C6—C5—H3	120.0	119.3	119.2	119.1	119.6
C1—C6—C5	121.2	120.1	120.0	120.1	119.7
C1—C6—H4	119.4	119.7	120.0	120.1	121.7
C5—C6—H4	119.4	120.1	119.9	119.7	118.5
O1—C7—C8	120.5	118.7	119.0	118.8	120.7
O1—C7—C4	120.7	119.8	120.0	119.7	121.4
C8—C7—C4	118.7	121.4	120.8	121.3	117.8
C9—C8—C7	122.3	125.6	125.2	125.0	123.3
C9—C8—H5	118.9	121.2	121.4	121.9	122.9
C7—C8—H5	118.9	112.5	112.8	112.5	113.6
C8—C9—C10	127.0	127.1	127.0	126.9	123.6
C8—C9—H6	116.5	118.1	118.1	118.6	121.3
C10—C9—H6	116.5	114.6	114.7	114.4	114.9

C11—C10—C15	117.6	117.9	117.9	118.1	119.7
C11—C10—C9	119.8	123.4	123.2	123.2	121.0
C15—C10—C9	122.5	118.6	118.7	118.5	119.2
C12—C11—C10	122.4	121.1	121.1	121.0	120.3
C12—C11—H7	118.8	118.7	118.6	118.5	119.6
C10—C11—H7	118.8	120.0	120.1	120.4	119.9
C13—C12—C11	117.8	119.3	119.4	119.4	118.7
C13—C12—H8	121.1	119.9	119.8	120.0	120.6
C11—C12—H8	121.1	120.6	120.7	120.5	120.6
C12—C13—C14	120.5	120.9	120.8	120.8	122.0
C12—C13—Cl1	118.7	119.4	119.4	119.4	119.0
C14—C13—Cl1	120.8	119.5	119.6	119. 6	118.9
C15—C14—C13	121.6	118.9	119.0	119.0	118.7
C15—C14—H9	119.2	120.8	120.8	120.6	120.7
C13—C14—H9	119.2	120.1	120.1	120.2	120.5
C14—C15—C10	120.1	121.6	121.5	118.8	120.3
C14—C15—H10	120.0	119.1	119.1	121.4	119.5
C10—C15—H10	120.0	119.2	119.3	119.6	120.0
C17—C16—C21	117.4	119.8	119.9	119.6	120.4
C17—C16—Se1	122.2	119.5	118.2	119.1	122.4
C21—C16—Se1	120.3	120.4	121.6	121.0	117.0
C18—C17—C16	121.4	120.0	119.9	120.1	119.6
C18—C17—H11	119.3	120.2	119.9	119.7	118.6
C16—C17—H11	119.3	119.7	120.0	120.1	121.6
C17—C18—C19	120.8	120.4	120.5	120.4	120.2
C17—C18—H12	119.6	119.4	119.3	119.1	120.3
C19—C18—H12	119.6	120.0	120.0	120.4	119.3
C20—C19—C18	117.6	118.9	118.9	119.0	119.6
C20—C19—C22	119.4	117.6	117.8	117.9	121.8
C18—C19—C22	123.0	123.1	123.0	122.8	118.4
C21—C20—C19	121.5	120.6	120.8	120.6	120.2
C21—C20—H13	119.3	120.8	120.6	120.2	119.5
C19—C20—H13	119.3	118.4	118.4	119.0	120.2
C20—C21—C16	121.3	119.9	119.7	120.0	119.7
C20—C21—H14	119.4	120.3	120.1	119.8	118.5
C16—C21—H14	119.4	119.6	120.1	120.1	121.7
O2—C22—C19	119.4	119.7	119.9	119.8	121.3
O2—C22—C23	120.2	118.8	119.1	118.8	120.6
C19—C22—C23	120.4	121.4	120.9	121.3	118.0
C24—C23—C22	123.3	125.6	125.2	125.0	123.4
C24—C23—H15	118.3	121.2	121.4	121.9	122.8
C22—C23—H15	118.3	112.5	112.7	112.6	113.5
C23—C24—C25	128.2	127.0	127.0	126.8	123.8

C23—C24—H16	115.9	118.2	118.1	118.6	121.2
C25—C24—H16	115.9	114.6	114.7	114.4	114.9
C26—C25—C30	117.6	117.9	117.9	118.1	119.6
C26—C25—C24	120.2	123.3	123.2	123.2	121.1
C30—C25—C24	122.2	118.7	118.8	118.6	119.1
C27—C26—C25	122.1	121.1	121.1	121.0	120.4
C27—C26—H17	118.9	118.7	118.6	118.5	119.5
C25—C26—H17	118.9	120.0	120.1	120.3	120.0
C28—C27—C26	119.0	119.3	119.4	119.4	118.7
C28—C27—H18	120.5	119.9	119.8	120.0	120.5
C26—C27—H18	120.5	120.6	120.6	120.5	120.6
C27—C28—C29	120.6	120.9	120.8	120.8	122.0
C27—C28—Cl2	120.1	119.4	119.4	119.4	119.0
C29—C28—Cl2	119.3	119.6	119.6	119.6	118.7
C30—C29—C28	120.0	118.9	121.5	119.0	118.7
C30—C29—H19	120.0	120.8	120.8	120.6	120.6
C28—C29—H19	120.0	120.1	120.1	120.2	120.5
C29—C30—C25	120.7	121.6	121.5	121.4	120.3
C29—C30—H20	119.7	119.1	119.1	118.9	119.5
C25—C30—H20	119.7	119.2	119.3	119.6	120.0

3.2. Electronic properties

To shed light on the electron transport capacity of the proposed compound by H. Bouraoui et al [21] (Figure 3), the study of electronic parameters such as the energy levels HOMO and LUMO and the energy gap [25] is very important and the obtained results at PM6, HF, DFT/B3LYPand DFT/ B3PW91methods with the same basis set 6-311G (d, p) are listed in Table 2.

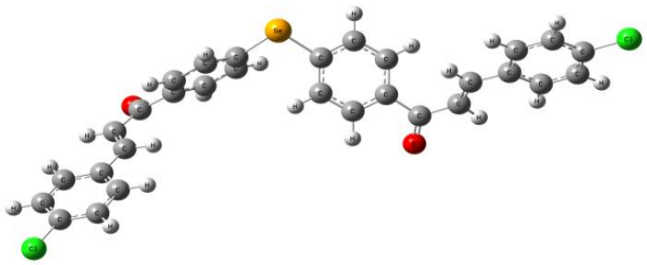

Figure 3. Optimized structure of the main molecule C30H20Cl2Se obtained by B3LYP/ 6-311G (d, p)

Table 2. ***Calculate energy values (HOMO, LUMO, Gap) (eV) of the compound studied by different methods***

	C30H20Cl2O2Se		
Methods	**E(HOMO) (eV)**	**E(LUMO) (eV)**	**Egap (eV)**
B3LYP	-6 .159	-2.548	3.611
B3PW91	-6.209	-2.594	3 .615
HF	-8.701	-1.306	7.395
PM6	-8.767	-1.134	7 .630

As shown in Table 2, the obtained values of HOMO and LUMO energies of theses studied molecules by different methods as PM6, HF, DFT/B3LYPand DFT/ B3PW91change significantly, the HOMOs are located at -8.767 eV, -8.701eV, -6.209 eV and -6.159 eV respectively. The LOMOs are located at -1.134 eV, -1.306 eV, -2.594 eV, and -2.548 eV respectively. Moreover, the energy gap decreases as follows: 7.630 eV > 7.395 eV > 3.615 eV > 3.611eV.

3.3. Proposed compounds

The strategy adopted consists of replacing the Selenium atom (Se) of the basic molecule (M0) proposed by H. Bouraoui et al with different atoms such as sulfur (S), oxygen (O), and nitrogen (N), then study their effect on the theoretically electronic properties, optical absorption. This strategy leads to the following structures M1, M2 and M3, as shown in Figure 4.

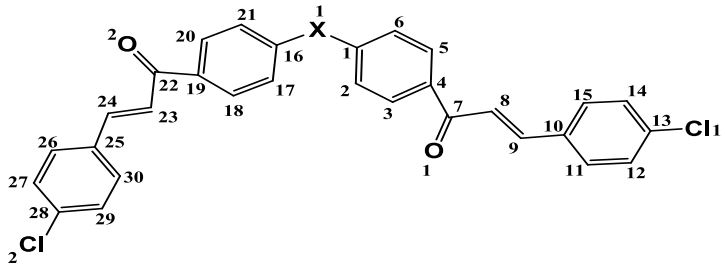

M_0: X= Se M_1: X=S M_2: X=O M_3: X=NH

Figure 4. Chemical structure for the proposed compounds M0, M1, M2 and M3

3.3.1. Ground-state geometries

To determine the geometrical parameters, the molecules M0, M1, M2, and M3 are fully optimized in their ground state using B3LYP/6-311G (d, p). All the optimized geometries for the studied compounds Mi are shown in Figure 5. Their selected geometrical parameters such as bond length, bond angle are collected in Table 3. The values of the optimized bond length of C-C, C-Cl, and C-O are nearly the same for all the compounds. Moreover, the values of the bond length C-Se, C-S, C-N, and C-O decreases as follows: 1.927 Å(C-Se) >1.790 Å(C-S) > 1.394(C-N) Å > 1.377 (C-O) Å. The values of the angle C - X - C of the studied compounds M0, M1, M2, and M3are 99.3°, 103.5°, 121.5°, and 130.1°respectively. This shows that the bond angles increase substantially from M0 to M3. Furthermore, the values of the angles X-C-C, C-C-C, Cl-C-C, O-C-C, H-C-C are nearly the same for all the compounds with a difference of 1 % or 2 %.

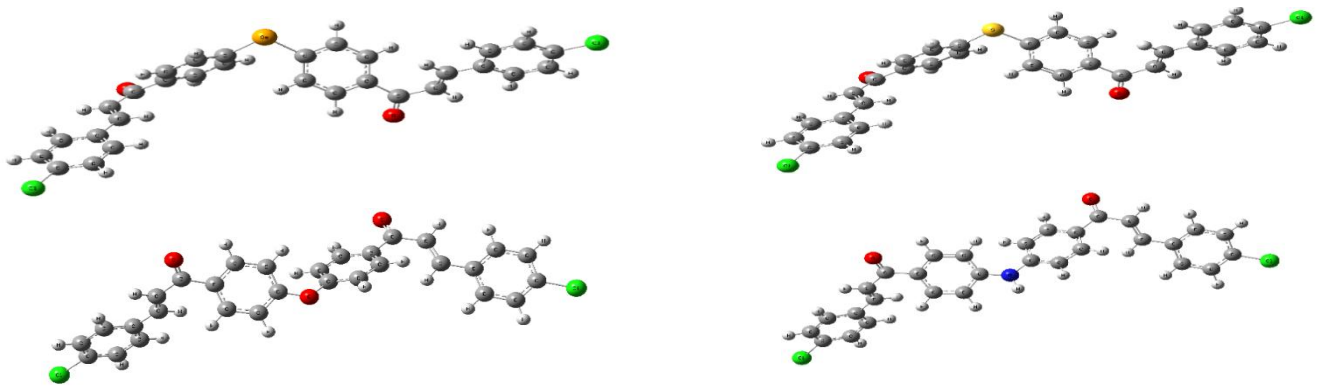

Figure 5. Optimized ground state structures for all studied compounds M0, M1, M2 and M3.

Table 3. ***Computed bond lengths (Å) and bond angles (°) of molecules M0, M1, M2 and M3 by DFT/ B3LYP (6-311G (d, p))***

Parameters	Se	S	O	NH
Bond length (Å)				
X—C1	1.927	1.790	1.377	1.394
X—C16	1.928	1.792	1.378	1.395
Cl1—C13	1.754	1.755	1.755	1.755
Cl2—C28	1.754	1.755	1.755	1.755
O1—C7	1.228	1.222	1.222	1.229
O2—C22	1.228	1.221	1.222	1.229
C1—C2	1.401	1.401	1.397	1.409
C1—C6	1.397	1.397	1.393	1.407
C2—C3	1.388	1.551	1.386	1.386
C3—C4	1.404	1.402	1.401	1.407
C4—C5	1.401	1.399	1.400	1.404
C4—C7	1.501	1.500	1.498	1.493
C5—C6	1.395	1.392	1.390	1.388
C7—C8	1.482	1.482	1.483	1.485
C8—C9	1.348	1.344	1.344	1.347
C9—C10	1.464	1.464	1.464	1.466
C10—C11	1.408	1.405	1.405	1.408
C10—C15	1.406	1.403	1.403	1.406
C11—C12	1.389	1.386	1.386	1.389
C12—C13	1.397	1.394	1.393	1.396
C13—C14	1.393	1.389	1.389	1.393
C14—C15	1.391	1.389	1.390	1.392
C16—C17	1.396	1.396	1.392	1.406
C16—C21	1.401	1.401	1.397	1.409
C17—C18	1.396	1.393	1.390	1.388
C18—C19	1.401	1.398	1.400	1.404
C19—C20	1.404	1.402	1.401	1.404
C19—C22	1.502	1.502	1.499	1.494
C20—C21	1.388	1.385	1.386	1.386
C22—C23	1.482	1.481	1.483	1.485
C23—C24	1.348	1.344	1.344	1.347
C24—C25	1.464	1.464	1.464	1.465
C25—C26	1.408	1.405	1.405	1.408
C25—C30	1.406	1.403	1.403	1.406
C26—C27	1.389	1.403	1.386	1.389
C27—C28	1.397	1.394	1.394	1.397
C28—C29	1.393	1.389	1.389	1.393
C29—C30	1.392	1.389	1.389	1.392
Parameters	Se	S	O	NH

Bond angles (°)				
C1—X—C16	99.3	103.5	121.5	130.1
C2—C1—C6	119.7	119.5	120.5	118.5
C2—C1—X	121.2	122.4	122.8	123.2
C6—C1—X	119.0	117.8	116.5	118.1
C1—C2—C3	119.9	119.9	119.2	120.0
C1—C2—H1	119.7	119.9	120.2	120.1
C3—C2—H1	120.2	120.0	120.5	119.7
C2—C3—C4	120.7	121.0	121.2	121.6
C2—C3—H2	120.8	120.5	120.4	120.2
C4—C3—H2	118.3	118.4	118.3	118.1
C5—C4—C3	118.8	118.6	118.5	117.9
C5—C4—C7	123.3	123.3	123.5	123.9
C3—C4—C7	117.6	117.8	117.8	117.9
C4—C5—C6	120.5	120.6	120.7	120.8
C4—C5—H3	120.0	120.1	120.1	120.0
C6—C5—H3	119.3	119.1	119.0	119.0
C1—C6—C5	120.1	120.1	119.6	120.8
C1—C6—H4	119.7	119.7	118.8	119.3
C5—C6—H4	120.1	120.0	121.4	119.8
O1—C7—C8	118.7	118.8	118.6	118.2
O1—C7—C4	119.8	119.9	120.0	120.2
C8—C7—C4	121.4	121.2	121.3	121.4
C9—C8—C7	125.6	125.7	125.7	125.7
C9—C8—H5	121.2	121.2	121.2	121.1
C7—C8—H5	112.5	112.4	112.4	112.5
C8—C9—C10	127.1	127.0	127.0	127.0
C8—C9—H6	118.1	118.2	118.3	118.2
C10—C9—H6	114.6	114.6	114.6	114.6
C11—C10—C15	117.9	117.8	117.8	117.8
C11—C10—C9	123.4	123.3	123.3	123.3
C15—C10—C9	118.6	118.8	118.8	118.7
C12—C11—C10	121.1	121.1	121.2	121.2
C12—C11—H7	118.7	118.6	118.6	118.7
C10—C11—H7	120.0	120.1	120.1	120.0
C13—C12—C11	119.3	119.3	119.3	119.3
C13—C12—H8	119.9	119.9	118.6	119.9
C11—C12—H8	120.6	120.6	120.6	120.6
C12—C13—C14	120.9	120.9	120.9	120.9
C12—C13—Cl1	119.4	119.4	119.4	119.4
C14—C13—Cl1	119.5	119.5	119.5	119.6
C15—C14—C13	118.9	118.9	118.9	118.9
C15—C14—H9	120.8	120.8	120.8	120.8

C13—C14—H9	120.1	120.1	120.1	120.1
C14—C15—C10	121.6	121.5	121.6	121.6
C14—C15—H10	119.1	119.0	119.0	119.1
C10—C15—H10	119.2	119.3	119.3	119.2
C17—C16—C21	119.8	119.6	120.5	118.5
C17—C16—X	119.5	118.3	116.5	118.2
C21—C16—X	120.4	121.8	122.7	123.1
C18—C17—C16	120.0	120.0	119.6	120.7
C18—C17—H11	120.2	120.1	121.4	119.8
C16—C17—H11	119.7	119.7	118.8	119.3
C17—C18—C19	120.4	120.6	120.7	120.8
C17—C18—H12	119.4	119.2	119.1	119.0
C19—C18—H12	120.0	120.1	120.1	120.0
C20—C19—C18	118.9	118.7	118.5	117.9
C20—C19—C22	117.6	117.8	117.8	118.0
C18—C19—C22	123.1	123.2	123.4	123.8
C21—C20—C19	120.6	120.9	121.2	121.6
C21—C20—H13	120.8	120.5	120.3	120.2
C19—C20—H13	118.4	118.4	118.3	118.1
C20—C21—C16	119.9	119.9	119.2	120.0
C20—C21—H14	120.3	120.1	120.5	119.7
C16—C21—H14	119.6	119.9	120.2	120.1
O2—C22—C19	119.7	119.8	120.1	120.3
O2—C22—C23	118.8	118.8	118.6	118.2
C19—C22—C23	121.4	121.2	121.2	121.4
C24—C23—C22	125.6	125.7	125.7	125.6
C24—C23—H15	121.2	121.3	121.2	121.1
C22—C23—H15	112.5	112.4	112.4	112.6
C23—C24—C25	127.0	127.1	127.1	127.1
C23—C24—H16	118.2	118.2	118.2	118.1
C25—C24—H16	114.6	114.6	114.5	114.6
C26—C25—C30	117.9	117.8	117.8	117.8
C26—C25—C24	123.3	123.3	123.3	123.3
C30—C25—C24	118.7	118.7	118.7	118.7
C27—C26—C25	121.1	121.1	121.2	121.2
C27—C26—H17	118.7	118.6	118.6	118.6
C25—C26—H17	120.0	120.1	120.1	120.0
C28—C27—C26	119.3	119.3	119.3	119.3
C28—C27—H18	119.9	119.9	119.9	119.9
C26—C27—H18	120.6	120.6	120.6	120.6
C27—C28—C29	120.9	120.9	120.9	120.9
C27—C28—Cl2	119.4	119.4	119.4	119.4
C29—C28—Cl2	119.6	119.5	119.5	119.5

C30—C29—C28	118.9	118.9	118.9	118.9
C30—C29—H19	120.8	120.8	120.8	120.8
C28—C29—H19	120.1	120.1	120.1	120.1
C29—C30—C25	121.6	121.6	121.6	121.6
C29—C30—H20	119.1	119.0	119.0	119.0
C25—C30—H20	119.2	119.3	119.3	119.2

3.4 Optoelectronic properties

To gain insights into the optoelectronic properties, the frontier molecular orbitals HOMO (Highest Occupied Molecular Orbital) and LUMO (Lowest Unoccupied Molecular Orbital) are determined. These orbitals inform us about the mode of interaction between molecular entities and provide a reasoı M1 ıalitative indication of the excitation propertie M0 ıe transport capacity of electrons or holes [26]. Therefore, the parameters (HOMO and LUMO) can be calculated from the optimized structures obtained by the method B3LYP / 6311G (d, p). So, We have determined for the four studied compounds M0, M1, M2, and M3the energy levels HOMO and LUMO and the energy band gap Egap = ELUMO – EHOMO [27]. These values are shown in Table 4.

Table 4. ***The HOMO, LUMO, and energy gap values (eV) of all the compounds calcu*** M2 ***the DFT/ B3LYP/6–311G (d, p) level*** M3

	B3LYP (6-311G (d, p))		
Compound	**E(HOMO) (eV)**	**E(LUMO) (eV)**	**Egap (eV)**
M0	-6 .159	-2.548	3.611
M1	-6.327	-2.549	3.778
M2	-6.610	-2.477	4.133
M3	-5.705	-2.477	3.515

Based on Table 4, the values of the HOMO / LUMO energies are respectively: -6 .159/-2.548 eV for M0, -6.327/-2.549 eV for M1,-6.610/-2.477 eV for M2 and -5.705/-2.477eV for M3. The values of Egap are 3.611 eV, 3.778 eV, 4.133, and 3.515 eV for M0, M1, M2, and M3 respectively. We note that this energy Egap decreases in the order M2 > M1 > M0 > M3. On the other hand, the examination of the highest occupied HOMO orbitals and the lowest virtual LUMO orbitals for the studied compounds is important because they can provide clear information on intramolecular load transfer (ICT) in such a system π-conjugated and the ability to transport electrons or holes [28]. Consequently, the electron density of HOMO and LUMO of the studied compounds obtained by B3LYP / 6-311G (d, p) is represented in Figure 6. From this figure, it is noted on the one hand that for all the compounds discussed, the electronic density of HOMO is essentially located on the atoms (Se, S, O, and N) and attached benzene rings, and on the other hand, the contribution to the LUMO is higher for the end groups of the molecule. In an electroluminescent device, our organic compounds have a bifunctional character that includes a hole-transporting (HTL) and emissive layer (EL) as described in the introduction. Noting that the migration of holes from the injection layer (HIL) to the transport layer (HTL) / (EML) often depends on the energy levels of the HOMO orbitals. Therefore, we consider the HOMO of the compounds and the materials in the connecting layers. In this work, we used poly (3, 4-ethylenedioxthiophene): poly (4 styrenesulfonate) (PEDOT: PSS) as HIL and used 2, 9- dimethyl-4, 7-diphenyl-1, 10-phenanthroline (BCP) as HBL for our electroluminescent devices [29]. The HOMO energy values of the studied compounds M0, M1, M2 and M3 calculated by B3LYP / 6-311 (d, p) are -6.159 eV, -6.327eV, -6.610eV and -5.705 eV respectively. The obtained results show that the HOMO energy levels of all compounds lie between that of PEDOT: PSS (-5.00 eV) and that of BCP (-6.50 eV) except HOMO levels for compound M2 (-6.610 eV) (see Figure 7).

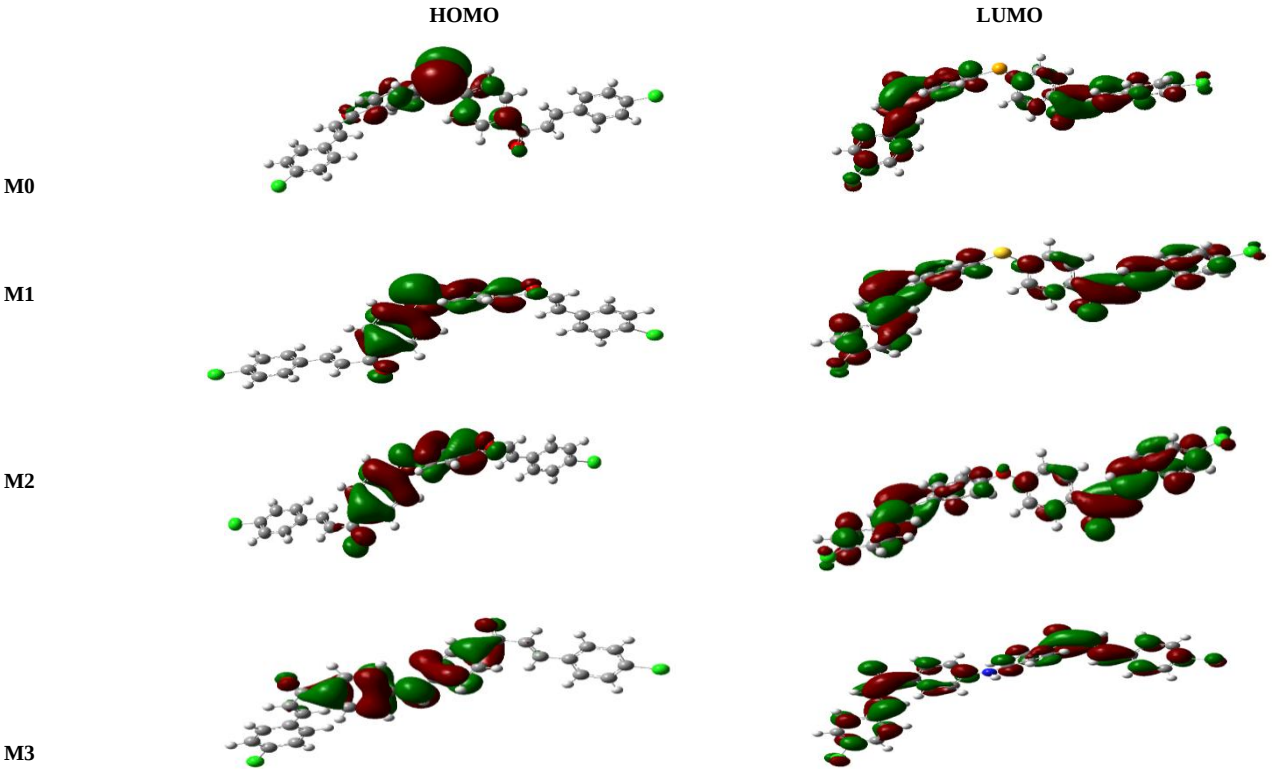

Figure 6. The contour plots of the HOMO and LUMO orbitals of the studied compounds

This indicates that the HOMO levels of all the studied compounds match with the ITO electrode use and facilitate the injection and transporting of holes.

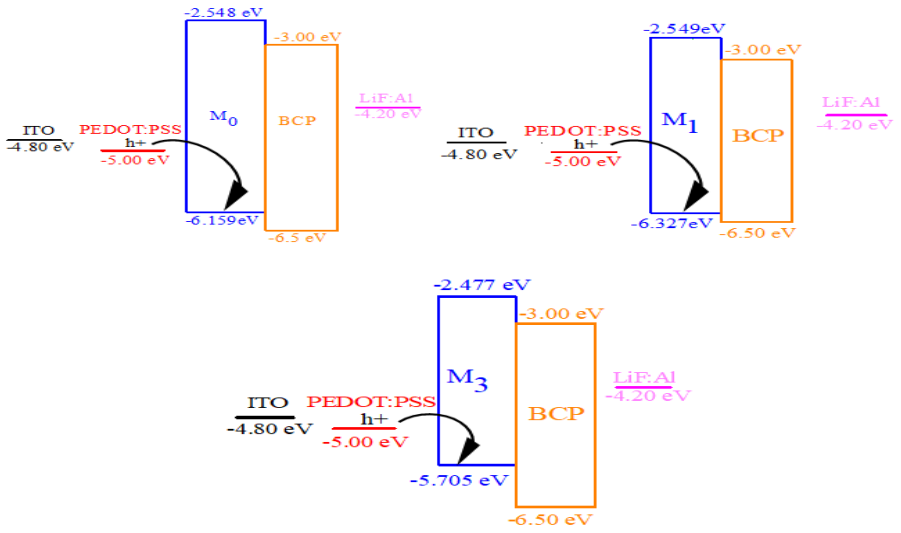

Figure 7. The configuration of three-layered OLEDs and the calculated energy diagrams of the studied compounds with the experimental values of PEDOT: PSS and BCP.

3.5 Ionization potentials, electron affinities and reorganization energies

The ionization potential (IP), the electronic affinity (EA), and the reorganization energy (λ) are the key performances of OLEDs devices, which can be used to evaluate the energy barrier of holes and electron injection including charge mobility and balanced charge [30]. It is well known that to have an easy injection of electrons (holes) into the emitting materials; they must have a high electron affinity and a low ionization potential. The electron affinity (EA) and the ionization potential (IP) of the compound Mi are calculated according to equations 1 and 2 [31]. The obtained results calculated at the B3LYP/6-311G (d, p) level are listed in Table 5.

$$PI = E^{+}(M_0) - E^{0}(M_0) \qquad (1)$$

$$EA = E^{0}(M_0) - E^{-}(M_0) \qquad (2)$$

E0 (M0): Energy in the neutral state

E+ (M0): Energy of cation obtained at ground state neutral molecule

E- (M0): Energy of anion obtained at ground state neutral molecule

Table 5. ***Ionization potential (IP eV), electron affinity (EA eV), reorganization energies for hole (λhole) and electron (λelectron) transport calculated at DFT/B3LYP/6-311G (d, p)***

Compounds Mi	IP	EA	λhole	λelectron	λTotal
M0	7.49	1.53	0.19	0.22	0.41
M1	7.57	1.54	0.21	0.22	0.43
M2	7.67	1.46	0.15	0.24	0.39
M3	7.24	1.42	0.26	0.23	0.46

From Table 5, the IP and EA changed with the alteration of the Chalcogen (O, S, and Se) and nitrogen (N) in the studied compound Mi. Indeed, the obtained values of the ionization potential (IP) decrease in the following order: M2> M1> M0> M3 indicating the increase of the hole injection from the HTL layer to the HOMO level of the studied compound. On the other hand, the compound M1 has the highest EA value (1.54 eV), indicating that it has a large electron-injecting capacity.

On the other side, the charge transport rate could be approximated by the Marcus electron-transfer theory with Equation (3) [32-33]:

$$K = A.\exp\left(\frac{-\lambda}{4K_B T}\right) \qquad (3)$$

Where A is a factor that depends on the strength of the electronic coupling between the emissive layer and the surface of the anode or cathode [34]. KB is the Boltzmann constant, T is the temperature and λ is the total reorganization energies.

For OLED materials, the carrier mobility for any organic material is based on the estimated reorganization energy [35]. Indeed, for efficient charge transport, the reorganization energy must be small [36]. Here, we calculated reorganization energies using the equation (4) [37], which are tabulated in Table 5 (using B3LYP functional with 6- 311G(d, p) basis set).

$$\lambda_i = \left[E^{\pm}(M_0) - E^{\pm}(M^{\pm})\right] - \left[E^{0}(M^{\pm}) - E^{0}(M_0)\right] \qquad (4)$$

Where E± (M0) is the energy of the cation (anion) calculated with the optimized structure of the neutral molecule, E± (M±) is the energy of the cation (anion) calculated with the optimized cationic (anionic) structure, E0 (M±) is the energy of the neutral molecule calculated at the cationic (anionic) state, and the E0 (M0) is the energy of the neutral molecule at the ground state (Illustration in Figure 8) [38].Through Table 5, the obtained values indicate that the

electron reorganization energies λe are slightly higher than those corresponding to the reorganization of the holes λh for all compounds except M3.The analysis of reorganization energy suggested that the studied compounds M0, M1, M2 are better for the transport of holes than the injection of electrons.

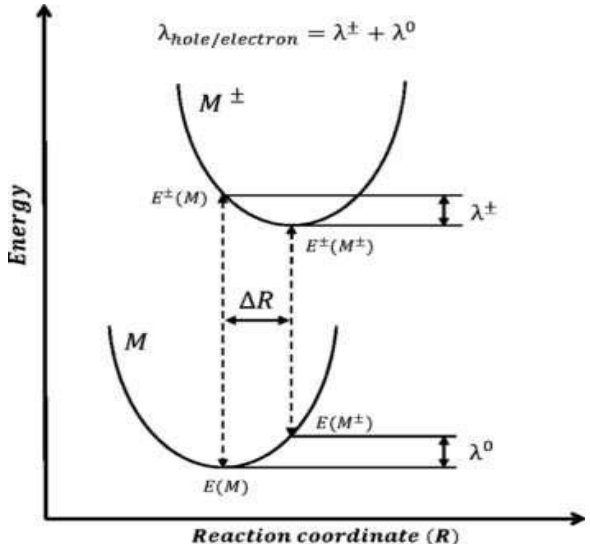

Figure 8. Energy plot against reaction coordinate (R) to illustrate reorganization energy calculations.

3.6. Chemical reactivity indices

Based on the theory of the limit molecular orbit (LMO), the reactivity indices can be defined on the basis of the energy difference between the HOMO and the LUMO [39]. Therefore, the calculations of the chemical reactivity indices [40] (the chemical potential (μ), chemical hardness (η), and electronegativity (χ)) have been carried out from the following relationships [41].

- Chemical potential $\mu = (EHOMO + ELUMO)/2$ (5)
- Chemical hardness $\eta = (ELUMO - EHOMO)/2$ (6)
- Electronegativity $-\chi = (EHOMO + ELUMO)/2$ (7)

Table 6. ***The HOMO, LUMO, energy gap values (eV) and chemical reactivity indices ((η), (μ), (χ)) for the studied compounds obtained at B3LYP/6-311G (d, p)***

Compounds Mi	E(HOMO) (eV)	E(LUMO) (eV)	Egap (ev)	μ	η	χ
M0	-6 .159	-2.548	3.611	-4.353	1.805	4.353
M1	-6.327	-2.549	3.778	-4.438	1.889	4.438
M2	-6.610	-2.477	4.133	-4.543	2.066	4.543
M3	-5.705	-2.477	3.515	-4.182	1.614	4.182

According to Table 6, the values of μ for the four compounds Mi, i = 0 to 3 indicate that the electronic chemical potential increase in the following order: M2 (-4.543) < M1 (-4.438) < M0 (-4.353) < M3 (-4.182). The values of η indicate that the compounds M0, M1, and M3 have the lowest value of hardness, i.e. 1.805, 1.889, and 1.614, respectively, compared to M2 (2.066) which means that these are soft molecules. Therefore, the compounds M0, M1, and M3 are more stable and more reactive compared to M2. In addition, the electronegativity values of the compounds M2, M1, M0, and M4 were found to be 4.543, 4.438, 4.353, and 4.182, respectively

3.7. Absorption Properties

To gain insights into the electronic transitions and excitation properties, of the four compounds, we performed calculations using the TD / B3LYP and TD / CAM-B3LYP quantum chemistry methods with the 6-311G (d, p) basis set on the optimized geometries. The parameters considered here are the electronic vertical transition energy (Eex), the maximum of absorption (λmax), the oscillator forces (f), and the nature of the transitions. These parameters are shown in Table 7.

Table 7. ***The first electronic vertical excitations were calculated using TD-B3LYP/6- 311G (d, p), TD- CAM-B3LYP/6-311G (d, p) method in the gas phase***

TD/B3LYP/6-311G (d, p)					TD- CAM-B3LYP/6-311G (d, p)				
Compounds	**λabs(nm)**	**Eex (eV)**	**O.S**	**MO/Character**	**Compounds**	**λabs(nm)**	**Eex (eV)**	**O.S**	**MO/Character**
M0	383.113	3.23	0.16	H>L (72%)	M0	299.940	4.14	1.16	H>L (52%)
M1	377.963	3.28	0.27	H>L (74%)	M1	296.539	4.18	1.39	H>L (48%)
M2	338.308	3.66	0.71	H>L (68%)	M2	285.386	4.34	1.74	H>L (26%)
M3	401.383	3.08	0.62	H>L (96%)	M3	318.412	3.39	1.36	H>L (56%)

Based on the UV-Vis absorption spectra shown in Figures 9 and 10, we observe the similar absorption behavior of the studied molecules (M0-M3). The vertical S0→S1 excitation energies based on the TD-B3LYP calculations for the optimal B3LYP geometries with the 6-311G (d, p) basis sets are 3.08 eV to 3.66 eV. The excitation energies obtained from the functional CAM-B3LYP are 3.39 eV to 4.34eV. We note that the vertical excitation energies shown in Table 7 using B3LYP functional lower than those obtained by CAM-B3LYP. In addition, as shown in Table 7 a typical difference from 50 to 83 nm between the wavelengths of absorption calculated by the TD- B3LYP and TD-CAM-B3LYP method in the gas phase. The maximum absorption values calculated for the four compounds M0, M1, M2, M3 using the TD- B3LYP are ranked respectively 383.113, 377.963, 338.308, and 401.383 nm. The maximum absorption values calculated for the four compounds M0, M1, M2, M3 using theTD-CAM-B3LYP are ranked respectively 299.940, 296.539, 285.386, and 318.412 nm. From Table 8, the main contribution of maximum absorption corresponds to the promotion of an electron from HOMO to LUMO, which is a transition π-π*.

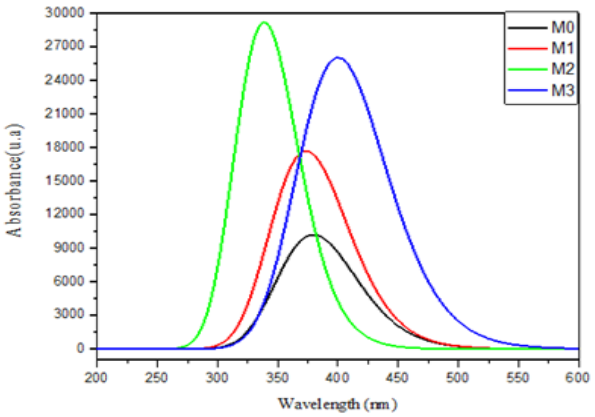

Figure 9. Absorption spectra of all compounds calculated using TD-B3LYP/6-311G (d, p)

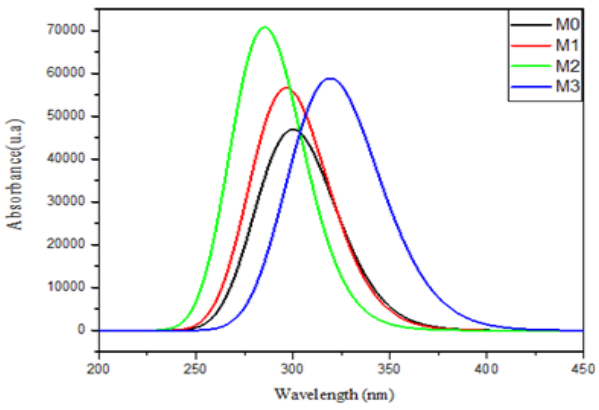

Figure 10. Absorption spectra of all compounds calculated using TD-CAM-B3LYP/6-311G (d, p)

3.8 Electrostatic potential

To predict physicochemical properties, the PPM is directly related to electron density and a very useful descriptor in the detection of sites for electrophilic and nucleophilic attack reactions, the interactions of hydrogen bonding as well as the electrostatic potential areas [42,43]. Therefore, the molecular electrostatic potential was evaluated using the B3LYP / 6-311G (d, p) method (Figure 11). We note that the MEP is a plot of electrostatic potential mapped into the constant electron density surface [44]. In general, regions rich in electrons (red) correspond to electrophilic reactivity, and regions deficient in electrons (blue) correspond to nucleophilic reactivity and green represents regions of zero potential [45]. The (MEP) map (Figure 11) shows that the maximum positive region of four compounds is located on the atoms of Selenium, Sulfur, Oxygen, Nitrogen, and phenylene rings (hydrogen and carbon atoms), which indicates that this area is a site of electron attraction (i.e. those areas where donating of a nucleophile is most favorable).On the other side, we also notice that the negative electrostatic potential region is mainly localized in the acceptor group (prop-2-en-1-one), which is a possible site for an electrophilic attack. Finally, the zone with zero potential is that where are the atoms of chlorine.

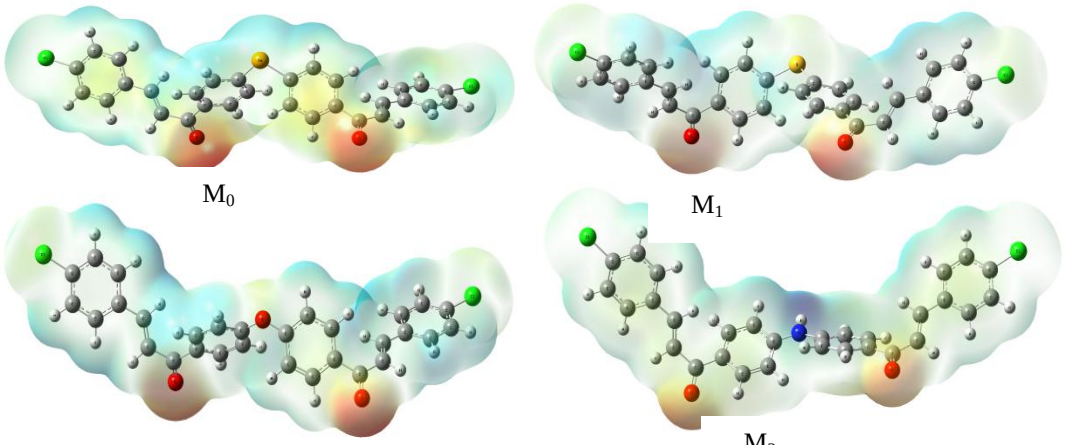

Figure 11. Electro ntial around the molecule using DFT/B3LYP/ 6-311G (d, p)

3. 9 Nonlinear optical (NLO) properties

Understanding of nonlinear optical properties is very important because of their potential applications in modern communication technology, data storage, telecommunication, and optical signal processing [46]. The molecules with delocalized electrons are getting much attention due to their large nonlinear optical properties. Indeed, the NLO properties of the base molecules are important to determine the NLO properties of the materials [47]. Therefore, DFT has been widely used to study NLO organic materials [48]. Properties, such as the dipole moment (μ), polarizability (αij), and first hyperpolarizability (βtot), are related to non-linear optical properties. Our derived values are summarized in Table 8.The equations used to derive the value of the total dipole moment (μtot), the average isotropic polarizability <α> and the first order of the hyperpolarizability (βtot), respectively, are the following [49].

$$\mu_{tot} = \sqrt{\mu_x^2 + \mu_y^2 + \mu_z^2} \quad (8)$$

$$\langle\alpha\rangle = \frac{1}{3}(\alpha_{xx} + \alpha_{yy} + \alpha_{zz}) \quad (9)$$

$$\beta_{tot} = \sqrt{\beta_x^2 + \beta_y^2 + \beta_z^2} \quad (10)$$

Here, $\beta_i = (i = x, y, z)$ combines the different quantities: $\beta_i = (\frac{1}{3})\Sigma j = x, y, z(\beta_{ijj} + \beta_{jij} + \beta_{jji})$ The NLO behavior of a molecule is usually determined by comparing the total dipole moment (μ_{tot}) and the average first-order hyperpolarizability (β_{tot}).

Table 8. ***The dipole moments μ, polarizability α, average isotropic polarizability <α> and the first hyperpolarizability βtot of M0-M3. The polarizability αij and hyperpolarizability tensors (βijj) have been converted into electronic units (esu) (α; 1 a.u = 0.1482×10^{-24}esu, β; 1 a.u = 8.6393×10^{-33}esu).***

Parameters	M0	M1	M2	M3
μx	0.8935	0.8476	0.6659	0.4996
μy	0.3240	0.8043	2.5779	4.3073
μz	-3.2190	-2.8877	-2.3468	-3.2877
μtot	3.3536	3.1151	3.5491	5.4416
αxx	724.194	718.537	684.810	755.828
αxy	-22.4663	-23.9045	-11.3996	3.197
αyy	323.351	318.482	322.787	378.514
αxz	-18.1333	-20.3035	21.5539	-1.77465
αyz	-11.1704	-9.86207	-25.8397	-33.7724
αzz	306.162	294.401	258.030	224.142
αtot(a.u)	451.236	443.806	421.87	452.828
α [10−24esu]	66.873	65.772	62.521	67.109
βxxx	2605.26	2577.86	1393.22	1096.72
βxxy	238.429	660.734	2050.06	2636.33
βxyy	-148.035	-1387.76	-692.159	-336.784
βyyy	583.883	666.668	616.061	784.342
βxxz	-2780.83	-2566.83	-1613.11	-2145.12
βxyz	-164.517	-281.656	-408.565	-391.381
βyyz	-351.928	-217.568	39.6687	49.5820
βxzz	-142.685	-176.817	-121.896	-331.271
βyzz	-10.7489	-42.4079	3.35078	-12.7189
βzzz	8.7226	60.9252	1.53783	27.8480
βtot(a.u)	3228.558	3177.303	3151.56	4009.144
β [10-33 esu]	27892.4811	27449.673	27227.272	34636.197

Table 8 shows that the values of average polarizability for the studied compounds M0, M1, M2, and M3 are 451.236 a.u, 443.806 a.u,421.87a.u, and 452.828 a.u respectively. Indeed, Average polarizability decreases across the studied molecules in the order: M3 > M0 > M1 > M2. We remark that the least value of average polarizability is attributed to compound M2 [421.87 (a.u)]. In addition, the comparison of μtot values of M0-M3 compounds indicated that μtot values decrease in the order: M3 > M2 > M0 > M1. The values of βtot for the set of molecules increase in the order M2 (3151.56 a.u) < M1 (3177.303 a.u) < M0 (3228.558 a.u) < M3 (4009.144 a.u). That is the hyperpolarizability increases in a manner compatible with the decrease in Egap. On the other hand, it was observed that the compound M3 with the nitrogen (N) provides the highest value of βtot (4009.144 (a.u)) among all compounds. This highest and lowest NLO response in the case of M3 and M2, respectively, can be attributed to the effective charge transfer from the donor to the acceptor.

Conclusion

In this paper, we investigated geometric structures, optoelectronic properties, intramolecular charge transfer (ICT), load mobility performance, absorption properties, electrostatic potential, and nonlinear optical (NLO) properties of the

four M0–M3 compounds using DFT and TD-DFT methods. The insertion of chalcogen O, S, Se, and nitrogen N affects the optoelectronic properties. They lead to a reduction of the HOMO-LUMO energy gaps and enhance intramolecular charge transfer (ICT).Our calculated results reveal that the studied compounds generally have prohibited band energies which make them good candidates for applications bifunctional OLED materials. The results of reorganization energies show that these compounds are better for the hole transporting material, this means that these compounds are better for carrying holes than electron injection and therefore can act as emitters in OLEDs. The calculated UV-vis absorption spectra of all compounds present at an electron excitation of the HOMO → LUMO level and an electronic transition of the type π–π* at approximately 400 nm. The first hyperpolarizability analysis reveals that the study compounds possess considerable NLO properties.

References

[1] Y. Karzazi, "Organic Light Emitting Diodes : Devices and applications", *J. Mater. Environ. Sci.*, 5 (2014) 1-12

[2] H. Derouiche, V. Djara, "Impact of the energy difference in LUMO and HOMO of the bulk heterojunctions components on the efficiency of organic solar cells", *J. Solar Energy Materials and Solar Cells*., 91 (2007)1163–1167.

[3] H. Spanggaard, F. C. Krebs, "A brief history of the development of organic and polymeric photovoltaics", *J. Solar Energy Materials and Solar Cells.*, 83 (2004) 125–146.

[4] N. Karl, "Charge carrier transport in organic semiconductors", *J. Synthetic Metals.*, 134 (2003) 649–657 2003.

[5] D.Braun, "Semiconducting polymer LEDs", *J. Materialstoday*., 5 (2002) 32-39.

[6] G.Li, V. Shrotriya, J.Huang, Y.Yao, T.Moriarty, K.Emery, Y. Yng, "High-efficiency solution processable polymer photovoltaic cells by self-organization of polymer blends", *J. nature materials.*, 4 (2005) 864-868.

[7] M. C. Hamilton, S. Member, S. Martin, "Thin-Film Organic Polymer Phototransistors", *J. IEEE Transaction on Electron Devices.*, 51 (2004) 877–885.

[8] H. Ebata, E. Miyazaki, T. Yamamoto, K. Takimiya, "Synthesis, Properties, and Structures of Benzo[1,2-b:4,5-b′]bis[b]benzothiophene and Benzo[1,2-b:4,5-b′]bis[b]benzoselenophene", *J. Organique Letters.* (2007) 2224–2226.

[9] H.Chen, Q.Cui, G.Yu, Y.Guo, J. Huang, M.Zhu, X.Guo, Y. Liu, "Synthesis and Characterization of Novel Semiconductors Based on Thieno [3 , 2- b][1] benzothiophene Cores and Their Applications in the Organic Thin-Film Transistors", *J. Phys. Chem.*,115 (2011) 23984 –23991.

[10] M.M. Azraina, M.R. Mansora, G. Omara, S.H.S.M. Fadzullaha, S.R. Esaa, L.M. Limd, D. Sivakumara, M.N.A. Nordina, "Effect of high thermal stress on the organic light emitting diodes (OLEDs) performances", *Synth. Met.*, 247 (2019)191–201.

[11] M. Raftani, T. Abram, R. Kacimi, M. N. Bennani, M. Bouachrine, "Organic compounds based on pyrrole and terphenyl for organic light-emitting diodes (OLED) applications : Design and electro-optical properties", *J. Journal of Materials and Environmental Sciences.*,11 (2020) 933–946.

[12] R. M. Christie, "Fluorescent dyes", *J.Woodhead Publishing Limited.*, 1 (2011) 562-587.

[13] C. W. Tang, S. A. Vanslyke, "Organic electroluminescent diodes", *J. Appl. Phys. Let.*, 12 (1987) 913-915.

[14] B. Lussem, M. Furno, K. Leo, "Highly effi cient pin- type OLEDs", *J.Woodhead Publishing Limited.*, (2013) 173-191.

[15] Y. Li, J.Y. Liu, Y.D. Zhao,Y.C. Cao, "Recent advancements of high efficient donor – acceptor type blue small molecule applied for OLEDs", J. Materialstoday.00 (2017) 1-9 .

[16] S.H. K.Park, M. Ryu, C. S. Hwang, S. Yang, C. Byun, J. k Lee, J. Shin, S.M. Yoon, H. Y. Chu, K. I. Cho, "42.3:Transparent ZnO Thin Film Transistor for the Application of High Aperture Ratio Bottom Emission AM-OLED Display", *J. The Society for Information Display.*, 39 (2008) 629–632.

[17] W. Brutting, J. Frischeisen, T. D. Schmidt, B. J. Scholz, C.Mayr, "Device efficiency of organic light-emitting diodes: Progress by improved light outcoupling", *J .Phys.Status Solidi A.*, 210 (2013) 44–65.

[18] A. Tripathi, C. Prabhakar, "Optical and charge transport properties of chalcogen (O, S and Se) based acene molecules", *J.*

Mol. Struct., 1203 (2019) 1-21.
[19] A. Tripathi, C. Prabhakar, "Impact of heteroatom (S and N) position and change in central ring of anthracene with heterocyclic ring on charge transport and optical properties in anthratetrathiazole (ATTz)", *J. Sulfur Chem.*, 40 (2019) 361–376.
[20] A. Tripathi, P. Chetti, "Enhanced charge transport properties in heteroatomic (NH, O, Se) analogs of benzotrithiophene (BTT) isomers: a DFT insight", *J. Mol. Simul.*, 46 (2020) 548–556.
[21] H. Bouraoui, Y. Mechehoud, S. Chetioui, R. Touzani, M. Medjani, A. Benmilat, "A. Boudjada, Crystal structure and Hirshfeld surface analysis of (2E,2′E)-1,1′-[selenobis(4,1-phenylene)]bis[3-(4-chlorophenyl)prop-2-en-1-one] ", *J. Acta Crystallogr. Sect. E Crystallogr. Commun.*, 75 (2019) 1724 –1728.
[22] N. Sundaraganesan, S. Ilakiamani, P. Subramani, B. Dominic Joshua, "Comparison of experimental and ab initio HF and DFT vibrational spectra of benzimidazole", *J. Spectrochimica Acta Part A.*, 67 (2007) 628-635.
[23] G. E. Frisch, M. J. Trucks, G. W. Schlegel, H. B, Scuseria, B. Robb, M. A. Cheeseman, J. R. Scalmani, G. Barone, V. Mennucci et al. "Gaussian 09." Wallingford. p. Revision A.02. 2009.
[24] S. Muthu, M. Prasath, R. A. Balaji, "Experimental and theoretical investigations of spectroscopic properties of 8-chloro-1-methyl-6-phenyl-4H-[1,2,4]triazolo[4,3-a][1,4]benzodiazepine", *J. Spectrochim. Acta - Part A Mol. Biomol. Spectrosc.*, 106 (2013) 129–145.
[25] Imelda, Emriadi, H. Aziz, A. Santoni, "Computational design of novel coumarin sensitizers to improve the efficincy of solar cells", *Mor. J. Chem.*, 10 (2022) 180-190.
[26] S. Boussaidi, A. Amkassou, H. Zgou, A. Eddiouan, Y. N. Mabkhot, A. Barakat, H. Chaib, T. Ben Hadda, "Theoretical study of organic materials based on Thieno[2,3-b]thiophene as layer of bulk heterojunction solar cells", *Mor. J. Chem.*, 5 (2017) 425-437
[27] A, Zahllou. T, Abram. S, Boussaidi. H, Zgou. L, Bejjit, M, Bouachrine," Theoreticalinvestigation of new organic materials based on fluorene and thiophene for photovoltaic applications", *Mor. J. Chem.*, 3 (2015) 861-871.
[28] Y. A. Sadiki, S.M Bouzzine, M. Bouachrinea, M. Hamidi, L. Bejjit, M. Elhaddad, F. Serein-Spirau, J.-P. Lère-Porte, J.-M. Sotiropoulos, "New organic compounds based on N-fluorene-carbazole moiety fordye-sensitized solar cells. Computational study", *Mor. J. Chem.*, 3 (2015) 108-121.
[29] A. M. Thangthong, D. Meunmart, N. Prachumrak, S. Jungsuttiwong, T. Keawin, T. Sudyoadsuk, V. Promarak, "Synthesis and characterization of 9,10-substituted anthracene derivatives as blue light-emitting and hole-transporting materials for electroluminescent devices", *J. Tetrahedron.*, 68 (2012) 1853–1861.
[30] A. Tripathi, P. Chetti, "Enhanced charge transport properties in heteroatomic (NH, O, Se) analogs of benzotrithiophene (BTT) isomers: a DFT insight", *J. Mol. Simul.*, 0 (2020) 1–9.
[31] A. Tripathi, P. Chetti, "Optoelectronic properties of benzotrithiophene isomers: A density functional theory study", *J.* Chinese Chem. Soc., 66 (2019) 1–8.
[32] R. A. Marcus, "Electron Transfer Reactions in Chemistry : Theory and Experiment (Nobel Lecture)", *J. Angewandte Chimie.*, 32 (1993) 1111-1222.
[33] P. F. Barbara, T. J. Meyer, M. A. Ratner, "Contemporary issues in electron transfer research", *J. Phys. Chem.* 100 (1996) 13148–13168.
[34] M. Bourass, N. Komiha, O. K. Kabbaj, N. Wazzan, M. Chemek, M. Bouachrine, "The photophysical properties and electronic structures of bis[1]benzothieno[6,7-: D:6′,7′- d ′]benzo[1,2- b:4,5- b ′]dithiophene (BBTBDT) derivatives as hole-transporting materials for organic light-emitting diodes (OLEDs) ", *New J. Chem.*, 43 (2019) 15899–1590.
[35] J.H. Pan, H.L.Chiu, L.Chen, B.C. Wang, "Theoretical investigations of triphenylamine derivatives as hole transporting materials in OLEDs: Correlation of the Hammett parameter of the substituent to ionization potential, and reorganization energy level", *J. Computational Materials Science.*, 38 (2006) 105–112
[36] A. Hlel, S. Ghomrasni, W. Taouali, K. Alimi, "Acceptor / Donor End Capped Phenylene-Thiophene Co-oligomers Toward Efficiencies Organic Electronic Devices", *J International Journal of Computational and Theoretical Chemistry.*, 8 (2020) 1–10,

2020.
[37] R. F. Jin, Y. F. Chang, "A theoretical study on photophysical properties of triphenylamine-cored molecules with naphthalimide arms and different π-conjugated bridges as organic solar cell materials", *Phys. Chem. Chem. Phys.*, 17 (2015) 2094 – 2103.
[38] M. Bourass, N. Komiha, O. K. Kabbaj, N. Wazzan, M. Chemek, M. Bouachrine, "The photophysical properties and electronic structures of bis[1]benzothieno[6,7- d :6′,7′- d ′]benzo[1,2- b :4,5- b ′]dithiophene (BBTBDT) derivatives as hole-transporting materials for organic light-emitting diodes (OLEDs) ", *New J. Chem.*, 43 (2019) 15899-15909.
[39] A. Barhoumi, M. El Idrissi, S. Bakkas, A. Zeroual, A. Tounsi, A. El Hajbi, "A DFT study of the mechanism and regioselectivity of the reaction between diethyl trichloro-methyl phosphonate and diphenyl methyl phosphinite", *Mor. J. Chem.*, 8 (2020) 830-840.
[40] P. K. Chattaraj, B. Maiti, "HSAB principle applied to the time evolution of chemical reactions", *J. Am. Chem. Soc.*, 125 (2003) 2705–2710.
[41] R. G. Pearson, "Absolute electronegativity and hardness correlated with molecular orbital theory", *Proc. Natl. Acad. Sci.*, 83 (1986) 8440–8441.
[42] E. Scrocco, J. Tomasi, "Electronic Molecular Structure, Reactivity and Intermolecular Forces: An Euristic Interpretation by Means of Electrostatic Molecular Potentials", *Advances in Quantum Chemistry.*, 11 (1978) 116-190.
[43] G. Shakila, H. Saleem, N. Sundaraganesan, "FT-IR, FT-Raman, NMR and U-V Spectral investigation : Computation of vibrational frequency, chemical shifts and electronic structure calculations of 1-bromo-4-nitrobenzene", *World Scientific News.*, 61 (2017) 150–185.
[44] R. Kacimi, M. Bourassa, T. Toupance, N, Wazzan, M. Chemek, A. El Alamy, L. Bejjit, K.Alimi, M. Bouachrine, "Computational design of new organic (D–π–A) dyes baseon benzothiadiazole for photovoltaic applications, especially dye-sensitized solar cells", *Res. Chem. Intermed.*, 46 (2020) 3247–3262.
[45] B.D. Ostojic, B. Stankovic, D S. Đordevic, "Theoretical study of the molecular properties of dimethylanthracenes as properties for the prediction of their biodegradation and mutagenicity", *J. Chemosphere.*, 111 (2014) 144-150.
[46] M.Usman Khan, M. Khalid, M. Ibrahim, A. A. C. Braga, M.Safdar, A. A. Al-Saadi, M.R. S. A. Janjua, "First Theoretical Framework of Triphenylamine − Dicyanovinylene- Based Nonlinear Optical Dyes: Structural Modi fi cation of π - Linkers", *J. Phys. Chem.*, 122 (2018) 4009−4018.
[47] M. Ramzan, S. A. Janjua, "Nonlinear optical response of a series of small molecules: quantum modifcation of π-spacer and acceptor". *J. Iranian Chemical Society.*,14 (2017) 2041–2054.
[48] M.Khalid, A.Ali, R. Jawaria, M.A. Asghar, S.Asim, M.U. Khan, R. Hussain, M.F. Rehman, C. J. Ennis, M. S. Akram, "First principles study of electronic and nonlinear optical properties of A–D–π–A and D–A–D–π–A configured compounds containing novel quinoline–carbazole derivatives", *J. RSC Adv.*, 10 (2020) 22273–22283.
[49] M. Karabacak, E. Yilan , "Molecular structure, spectroscopic (FT-IR, FT-Raman, 13C and 1H NMR, UV), polarizability and first-order hyperpolarizability, HOMO and LUMO analysis of 4_-methylbiphenyl-2-carbonitrile", *Spectrochimica Acta Part A.*, 87 (2012) 273–285.